Food & Function

ROYAL SOCIETY OF CHEMISTRY

PAPER

View Article Online
View Journal | View Issue

Cite this: *Food Funct.*, 2025, **16**, 2316

Dietary phytosterol supplementation mitigates renal fibrosis *via* activating mitophagy and modulating the gut microbiota

Fan Yang,[a,b,c] Yingjie Gao,[a,b] Siyi Xie,[a,b] Wenjing Yang,[a,b] Qiyan Wang,[a,b,c] Wenqian Ye,[a,b] Lu Sun,[a,b] Jiangtao Zhou*[a,b] and XiuE Feng *[a,b]

Chronic kidney disease (CKD) poses a significant global health challenge, primarily driven by renal fibrosis, with limited treatment options. Addressing this condition necessitates either targeted medical treatments or dietary interventions. Phytosterols (PS) are cholesterol-like bioactive compounds in various plant-based foods with antioxidant and anti-inflammatory effects. A CKD mouse model was established using folic acid (FA) and treated with dietary supplements of two PS, stigmasterol (Stig) and β-sitosterol (β-Sito). The effects and mechanisms of PS were investigated through biochemical indices, pathology, transcriptomics, and 16S rDNA sequencing. The results indicated that high-dose PS are more effective than low-dose PS and Losartan potassium (LP) in reducing renal fibrosis, restoring function, and modulating oxidative stress and inflammation, with no significant differences between high-dose Stig and β-Sito treatments. Gene Ontology (GO) enrichment analysis revealed that PS were significantly enriched in pathways related to the mitochondrial outer membrane, ubiquitin-protein ligase binding, and other cellular components and molecular processes. PS reduced the expression of TGF-β/Smad and cGAS/Sting1/TBK1 and activated PINK1/Parkin pathway proteins, thereby mitigating renal fibrosis in mice. CKD is often associated with imbalanced gut microbiota and compromised intestinal barriers. Our observations indicated that PS restored the intestinal barrier, altered the composition of the gut microbiota, and improved renal function in CKD mice. The present findings indicate that both Stig and β-Sito activate mitophagy *via* the PINK1/Parkin pathway and modulate the gut microbiota, thereby alleviating renal fibrosis. The findings provide solid and significant implications for developing effective application of PS supplementation in the management of CKD, presenting novel concepts and approaches for research and clinical treatment.

Received 5th December 2024,
Accepted 11th February 2025

DOI: 10.1039/d4fo06043a

rsc.li/food-function

1. Introduction

Renal fibrosis is the primary driver of CKD progression to end-stage renal disease (ESRD).[1] Studies have demonstrated that renal fibrosis is closely linked to epithelial–mesenchymal transition (EMT).[2] Persistent kidney injury triggers EMT, leading to the transformation of multiple cell types, such as fibroblasts, glomerular cells, and tubular epithelial cells. Transforming growth factor-beta (TGF-β) activates pathways like Smad, converting renal tubular epithelial cells into fibroblasts.[3] TGF-β also enhances fibroblast proliferation and collagen production, exacerbating renal fibrosis. Since fibrosis is generally irreversible, inhibiting its progression is considered an effective strategy for preventing CKD.[4,5]

Mitophagy, the selective degradation of mitochondria through autophagy, plays a crucial role in eliminating damaged mitochondria and maintaining mitochondrial homeostasis.[6,7] Research has shown that CKD mice exhibit impaired autophagy. Recent studies have increasingly linked mitophagy levels to organ fibrosis progression, with dysregulated mitophagy recognized as a contributing factor to fibrosis pathogenesis.[8,9] Therefore, targeting mitophagy pathways offers a potential therapeutic strategy for slowing CKD progression. The gut microbiota plays a vital role in human health by producing nutrients and metabolites, coexisting harmoniously with the host.[10] CKD and intestinal microecology are interrelated and mutually influential.[11] CKD disrupts intestinal balance, damaging the mucosal barrier, reducing beneficial bacteria, and increasing harmful ones.[12] Conversely,

[a]*School of Pharmacy, Shanxi Medical University, Taiyuan, Shanxi province, China. E-mail: xiuefeng@sxmu.edu.cn, zjt881206@sxmu.edu.cn*
[b]*Medicinal Basic Research Innovation Center of Chronic Kidney Disease, Ministry of Education, Shanxi Medical University, Taiyuan, Shanxi province, China*
[c]*Shanxi Key Laboratory of Innovative Drug for the Treatment of Serious Diseases Basing on the Chronic Inflammation, College of Traditional Chinese Medicine and Food Engineering, Shanxi University of Chinese Medicine, Taiyuan, Shanxi province, China*

intestinal imbalances allow toxins to enter the bloodstream through the compromised barrier, triggering inflammation and worsening kidney damage in CKD patients. This creates a harmful cycle between the kidneys and intestines, leading to poor outcomes. Modulating the intestinal microbiota and its metabolites may represent a promising strategy for mitigating CKD.[13,14] Thus, altering the gut microbial ecosystem to improve renal dysfunction is a potential therapeutic strategy. Recent studies have shown that there is a complex interaction between the gut microbiota and mitochondrial dysfunction. A healthy gut microbiota can regulate host metabolism and promote mitophagy through metabolites like short-chain fatty acids, thereby protecting renal cells from oxidative stress and reducing chronic inflammation. Conversely, an imbalance in the gut microbiota may inhibit mitophagy and exacerbate renal oxidative damage.[15,16]

Functional foods and nutritional interventions are increasingly being recognized as potential therapeutic agents for the management of chronic diseases.[17,18] Phytosterols are naturally occurring bioactive compounds that are predominantly found in various plant-based foods, including but not limited to corn (*Zea mays*), sunflower seeds (*Helianthus annuus*), walnuts (*Juglans regia*), almonds (*Prunus amygdalus*), wheat (*Triticum aestivum*), mulberry fruit (*Fructus Mori*), Chinese yam (*Corni Fructus*) and ginseng (*Radix Ginseng*). Ginseng, wheat, sunflower seeds, almonds, walnuts, and corn are notably rich in PS, with concentrations reaching up to 45.95 g kg^{-1}, 4.13 g kg^{-1}, 2.89 g kg^{-1}, 1.99 g kg^{-1}, 1.77 g kg^{-1}, and 1.43 g kg^{-1}, respectively.[19,20] Common phytosterols, such as stigmasterol and β-sitosterol, as well as those present in rapeseed oil, exhibit structural and functional similarities to cholesterol. Recent studies indicate that PS effectively lower cholesterol and regulate lipids, potentially due to their impact on *in vivo* metabolism and interaction with nuclear receptors.[21,22] Phytosterols have been shown to possess a range of biological activities, including antioxidation, anti-inflammation, and lipid metabolism modulation. Abnormal lipid metabolism is frequently linked to the progression of CKD. By modulating lipid levels, phytosterols may alleviate renal burden and potentially decelerate disease progression.[23] Furthermore, experiments suggest that phytosterols have anti-inflammatory and antioxidant effects, which could be vital in treating kidney conditions like lupus nephritis, diabetic nephropathy, and hyperuricemia.[24–26] By reducing inflammation and oxidative stress, phytosterols may protect kidney cells and enhance kidney function. Experiments suggest that phytosterols have anti-inflammatory and antioxidant effects, which may help protect renal cells and enhance kidney function by reducing inflammation and oxidative stress, key factors in CKD progression. Based on these findings, it is hypothesized that dietary supplementation with phytosterols may contribute to the alleviation of CKD.

In this study, we selected stigmasterol and β-sitosterol, the two principal components of PS, to examine their potential in mitigating renal fibrosis. We also aimed to explore whether their mechanism of action involves the regulation of the PINK1/Parkin-mediated mitophagy pathway and the modulation of the gut microbiota. The study establishes a connection between PS supplementation and the reduction of renal fibrosis, primarily through the activation of mitophagy and the modulation of the gut microbiota. These findings propose PS as a promising candidate for therapeutic intervention, potentially suitable for dietary supplementation, and are anticipated to offer a theoretical foundation for the effective application of PS supplementation in the management of CKD.

2. Materials and methods

2.1 Chemicals and reagents

Folic acid (FA, CAS: 59-30-3, F7876-1G) was purchased from Sigma. Stigmasterol (CAS: 83-48-7, purity ≧ 95%), β-sitosterol (CAS: 83-46-5, purity ≧ 95%), and losartan potassium (CAS: 124750-99-8, purity ≧ 98%) were purchased from Yuanye Bio-Technology Co., Ltd. Assay kits for blood urea nitrogen (BUN, C013-2-1), creatinine (CRE, C011-2-1), urinary protein concentration (PRO, C035-2-1), malondialdehyde (MDA, A003-1), superoxide dismutase (SOD, A001-3), and reduced glutathione (GSH, A006-2-1) were purchased from Nanjing Jiancheng Bioengineering Institute. Antibodies for α-SMA (A17910, 1 : 5000), Smad3 (A191115, 1 : 5000), P-Smad2 (AP0269, 1 : 1000), P-Smad3 (AP0727, 1 : 2000), cGAS (A8335, 1 : 1000), TBK1 (A3458, 1 : 2000), P62 (A19700, 1 : 1000), GAPDH (A19056, 1 : 5000), β-actin (AC016, 1 : 10 000), and β-Tubulin (A12289, 1 : 5000) were purchased from Abclonal. Antibodies for COL-1 (67288-1-Ig, 1 : 5000), TGF-β1 (21898-1-AP, 1 : 3000), Smad2 (12570-1-AP, 1 : 5000), Smad7 (25840-1-AP, 1 : 2000), Sting1 (19851-1-AP, 1 : 2000), PINK1 (23274-1-AP, 1 : 1000), Parkin (14060-1-AP, 1 : 2000), and LC3 (14600-1-AP, 1 : 2000) were acquired from Proteintech. Antibody for FN1(ab199056, 1 : 3000) was purchased from Abcam. Enhanced RIPA lysate (AR0102-100) was sourced from Boster Biological Technology Co. Ltd. Trizol (Mei5bio, MF034) and RT-qPCR reagents (F166-plus-01 and MF787-01) were purchased from Mei5bio.

2.2 Animals

For this study, SPF grade C57BL/6 male mice (18–20 g, 6–8 weeks old) were obtained from Beijing Sibeifu Biotechnology Co., Ltd (animal license no. SCXK – (Jing) 2019–0010). Mice were grouped and raised in independent animal cages in SPF-level rooms, with an ambient temperature of 21 °C to 23 °C, with 35% to 65% humidity, and fed sterilized regular feed and water, and the they ate freely. All experimental protocols were reviewed and approved by the Ethics Committee of the China Institute for Radiation Protection, Taiyuan, China (License No. CIRP-IACLLC-(R)2024020).

2.3 Animal experiments

Mice were randomly assigned to seven groups (10 mice in each group): control group (CON), model group (FA), stigmasterol-50 mg kg^{-1} d^{-1} group (FA + Stig-L), stigmasterol-100 mg kg^{-1} d^{-1} group (FA + Stig-H), β-sitosterol-50 mg kg^{-1} d^{-1} group (FA

+ β-Sito-L), β-sitosterol-100 mg kg^{-1} d^{-1} group (FA + β-Sito-H) and Losartan potassium-10 mg kg^{-1} d^{-1} group (FA + LP) (Losartan potassium: a clinical adjunct to the treatment of chronic kidney disease). After one week of acclimatization feeding in the animal room, the CKD mouse model was established *via* a single intraperitoneal injection of 250 mg kg^{-1} FA solution.[27,28] After 7 days of modeling, the PS and LP groups received the specified doses of PS and LP (dissolved in 0.5% CMC-Na solution, doses of 50 mg kg^{-1} and 100 mg kg^{-1} of stigmasterol and β-sitosterol in CMC-Na solution were 5 mg mL^{-1} and 10 mg mL^{-1}, respectively, with a 30 g mouse gavaged with a volume of 0.3 mL) daily around 10 : 00 am, while the CON and FA groups received an equivalent volume of 0.5% CMC-Na solution, and the gavage was continued for 21 days. Throughout the feeding period, the body weights and food intake of each group were systematically recorded weekly. On day 28, mice were sacrificed by inhalation of isoflurane. Serum, urine, and kidney tissues were rapidly collected and stored at −80 °C for subsequent analysis. The fecal samples were collected in sterilized Eppendorf tubes and promptly stored at −80 °C to facilitate subsequent analysis of the gut microbiota.

2.4 Determination of PS and LP dosage in animal experiments

The doses of stigmasterol, β-sitosterol, and Losartan potassium were determined based on the existing literature and previous studies; to determine the intervention dose of PS, we reviewed animal studies on their effects in hyperuricemia, colitis, and acute lung injury. The most commonly used doses were 50 mg kg^{-1} d^{-1} and 100 mg kg^{-1} d^{-1}, both of which have shown a good remission effect on the disease.[5,7,29,30] The process of translating a human clinical dose to an equivalent animal dose can be accomplished by utilizing the established principles of interspecies drug dose conversion (human clinical dose : animal dose = 1 : 12.3).[31] By dose conversion, a mouse dose of 100 mg kg^{-1} d^{-1} is equivalent to a human dose of 8.108 mg kg^{-1} d^{-1}, which means that a 60 kg adult takes 486.48 mg of phytosterols per day; the dosage of PS is below the recommendations outlined by the American Heart Association, the National Cholesterol Education Program, and the Commission Regulation (European Union).[32–34] Therefore, the appropriate dose of PS in the present study was ultimately designated as the low dose of PS at 50 mg kg^{-1} day^{-1} and the high dose at 100 mg kg^{-1} day^{-1} for oral administration.

2.5 Histopathologic observation of the kidneys

The kidneys fixed in paraformaldehyde for 24 hours were then embedded in paraffin, dehydrated in ethanol, and cleared with xylene. Using a microtome, kidney tissue blocks were sliced into 3 μm sections. These sections were stained with Masson and hematoxylin–eosin (HE) for examination under a light microscope.

2.6 Transmission electron microscopy (TEM)

Kidney slices were post-fixed with 1% osmium tetroxide after initial fixation with glutaraldehyde. Before embedding in Spurr resin, the samples were dehydrated using acetone. Following sectioning with an ultramicrotome, slices were stained with lead citrate and uranyl acetate. Kidney ultrastructure images were captured using a transmission electron microscope (HT7800, HITACHI, Japan). The images were then analyzed to assess organelle changes and mitochondrial damage in kidney tissue.

2.7 RNA-sequencing analysis

Total RNA was extracted using the TRIzol reagent, and its integrity was assessed through agarose gel electrophoresis and the Agilent 2100 Bioanalyzer (Agilent Technologies, Palo Alto, CA, USA). RNA libraries were sequenced using the Illumina HiSeq™ 2500/4000 platform. Differential expression analysis of RNA between the groups was performed using DESeq2 software. The total number of differentially expressed genes (DEGs), as well as upregulated and downregulated genes, was quantified and analyzed using DESeq2/EdgeR. Selection criteria for genes included $|\log 2 \text{ Fold Change}| > 1$ and p-value < 0.05. Further bioinformatics analysis was performed on the identified DEGs.

2.8 Quantitative real-time PCR analysis

Total RNA was extracted from kidney tissues using the TRIzol reagent. RNA was reverse transcribed into cDNA using the PrimeScript™ RT reagent kit with gDNA Eraser (Takara, Beijing, China). qPCR was conducted using SYBR Green Supermix (EZB, Roseville, USA) and detected on a LightCycler 480 II system (Roche, Indiana, USA). Primer sequences used in the qPCR experiment are listed in Table 1, with all primers designed and synthesized by Sanggon Biotech. The comparative threshold cycle (C_t) method was used to determine the relative expression levels of target mRNAs, with GAPDH as the reference gene for normalizing the C_t values. (qPCR protocol: holding stage: 1 cycle, 95 °C, 30 s. Cycling stage: 40 cycles, 95 °C for 3 s, 60 °C for 30 s. Melt curve stage: 1 cycle, 95 °C for 15 s, 60 °C for 60 s, 95 °C for 15 s.)

2.9 Western blot

Kidney tissues were lysed with RIPA buffer, protein levels were quantified using the BCA assay, and 20 μg of protein was loaded for SDS-PAGE. After separation, proteins were transferred to PVDF membranes and blocked with 5% BSA for two hours at room temperature. Membranes were incubated overnight at 4 °C with the primary antibody, followed by one hour at room temperature with appropriate secondary antibodies, and then washed three times with TBST. Lastly, membranes were exposed to ECL solution, photographed, and analyzed using ImageJ for gray-level analysis.

2.10 Genomic DNA extraction and 16S-rRNA sequencing of feces

Colonic contents were collected and submitted to Applied Protein Technology Co., Ltd (Shanghai, China) for detection. Genomic DNA was extracted using the OMEGA DNA Kit, and its concentration and purity were assessed. The V3–V4 variable

Table 1 Primer sequences for quantitative real-time PCR amplification

Gene	Forward primers (5′–3′)	Reverse primer (5′–3′)
α-SMA	GCGTGGCTATTCCTTCGTGACTAC	CGTCAGGCAGTTCGTAGCTCTTC
COL-1	TGACTGGAAGAGCGGAGAGT	GTTCGGGCTGATGTACCAGT
FN1	GAAGTCGCAAGGAAACAAGC	GCATCGTAGTTCTGGGTGGT
TGF-β	ACCGCAACAACGCCATCTATGAG	GGCACTGCTTCCCGAATGTCTG
Smad2	GTCGTCCATCTTGCCATTCACTCC	GCTCTCCACCACCTGCTCCTC
Smad3	AGACGCCAGTTCTACCTCCAGTG	GCCAGCAGGGAAGTTAGTGTTCTC
Smad7	CAGCCGCCCTCGTCCTACTC	ACAGCAACACAGCCTCTTGACTTC
TNF-α	CCACCACGCTCTTCTGTCTACTG	TGGTTTGTGAGTGTGAGGGTCTG
IL-1β	CTCGCAGCAGCACATCAACAAG	CCACGGGAAAGACACAGGTAGC
IL-6	TTCTTGGGACTGATGCTGGTGAC	CTGTTGGGAGTGGTATCCTCTGTG
IL-10	TCCCTGGGTAGAAAGCTGAAGAC	CACCTGCTCCACTGCCTTGC
cGAS	GCTAAAGAAGGTGCTGGACAAATTG	CTTTGAACTCCGACTCCCGTTTC
Sting1	GATCGGCTTGAGCAGGCTAAAC	TAGACAATGAGGCGGCAGTTATTTC
TBK1	GGAACAACTCAATACCTGAGGACTG	GCAGGCGTAGCACACAACC
PINK1	GAGGAGAAGCAGGCGGAAGG	TCGCAGCATCGAGTGTCCAG
Parkin	TTGACACGAGTGGACCTGAGC	ACCTCTGGCTGCTTCTAGATCC
LC3I	CGCCGCCTGCAACTCAAC	CGTCTTCATCCTTCTCCTGTTCATAG
LC3II	GCGGGTGATTATAGAGCGATACAAG	GCGGGTGATTATAGAGCGATACAAG
P62	GCCGCCCTTGCCCTACAG	ATCAATGTCAACCTCAATGCCTAGAG
GAPDH	GGTTGTCTCCTGCGACTTCA	TGGTCCAGGGTTTCTTACTCC

regions were amplified by PCR using specific primers with barcodes and high-fidelity DNA polymerase, based on the selected sequencing regions. Target fragments were excised, purified, and analyzed by electrophoresis on 2% agarose gels. PCR products were quantified using a microplate reader fluorescent quantitative system, based on the initial electrophoresis results. Ratios were adjusted according to the sequencing requirements for each sample. The library was constructed using the TruSeq Nano DNA LT Library Prep Kit (Illumina). After a thorough quality check, the library was sequenced following analysis with the Agilent Bioanalyzer 2100 and Promega QuantiFluor.

2.11 Statistical analysis

Data were analyzed using GraphPad Prism 8.0.2 (CA, USA). The one-way analysis of variance (ANOVA) was used for comparisons among multiple groups, and Tukey's multiple comparisons test was used to correct for multiple comparisons. Results are presented as mean ± standard deviation (SD), with $p < 0.05$ considered statistically significant.

3. Results

3.1 PS ameliorated FA-induced kidney injury in CKD mice

To assess the impact of PS on CKD, a CKD mouse model was established as previously described.[27,28] The diagram of the animal experiments is shown in Fig. 1B. Kidney tissue, serum, small intestine, and colon contents were collected on day 28. After FA intervention, body weight and food intake in all groups, except the CON group, decreased significantly in the first three days and then gradually recovered (Fig. 1C and D). Clinical observations indicated that compared with the CON group, the kidney tissues in the FA group exhibited a paler color, smaller volume, lighter mass, and distinct granularity (Fig. 1E–G). Histopathological results showed multifocal atrophy of renal tubules, watery degeneration of epithelial cells, cell swelling, extensive connective tissue hyperplasia, and lymphocyte infiltration in the kidney tissue of FA-induced CKD mice (Fig. 1H). Following PS and LP intervention, the kidney index and weight increased, the color darkened, and histopathological improvements were observed (Fig. 1E–H). These findings suggest that PS effectively alleviate kidney injury in CKD mice in a dose-dependent manner.

3.2 PS improved renal function in CKD mice by regulating oxidative stress and inflammatory factors

To investigate the effects of PS on renal function, oxidative stress, and inflammatory factors in CKD mice, serum, urine, and kidney tissue supernatants were analyzed. CRE, BUN, and PRO are key indicators of renal function, with elevated levels indicating renal impairment.[2–4] The results indicated that the Stig-L, Stig-H, β-Sito-L, β-Sito-H and LP groups significantly reduced the levels of CRE, BUN, and PRO in a concentration-dependent manner compared to the FA group (Fig. 2A). Oxidative stress and inflammation are critical processes driving CKD progression, interacting to cause pathological changes.[6,7] Compared to the FA group, the Stig-H and β-Sito-H groups significantly elevated levels of SOD and GSH, as well as reduced levels of MDA, outperforming the positive drug LP group (Fig. 2B). RT-qPCR results demonstrated that pro-inflammatory factors (IL-6, IL-1β, TNF-α) were markedly reduced, while anti-inflammatory factor IL-10 was significantly elevated in the PS group and the LP group compared to the FA group (Fig. 2C). In summary, PS and LP intervention reduced CRE, BUN, and PRO levels, decreased MDA levels, and increased SOD and GSH levels. Additionally, pro-inflammatory factor levels were reduced, and anti-inflammatory factor levels increased (Fig. 2A–C). These findings indicate that PS improve

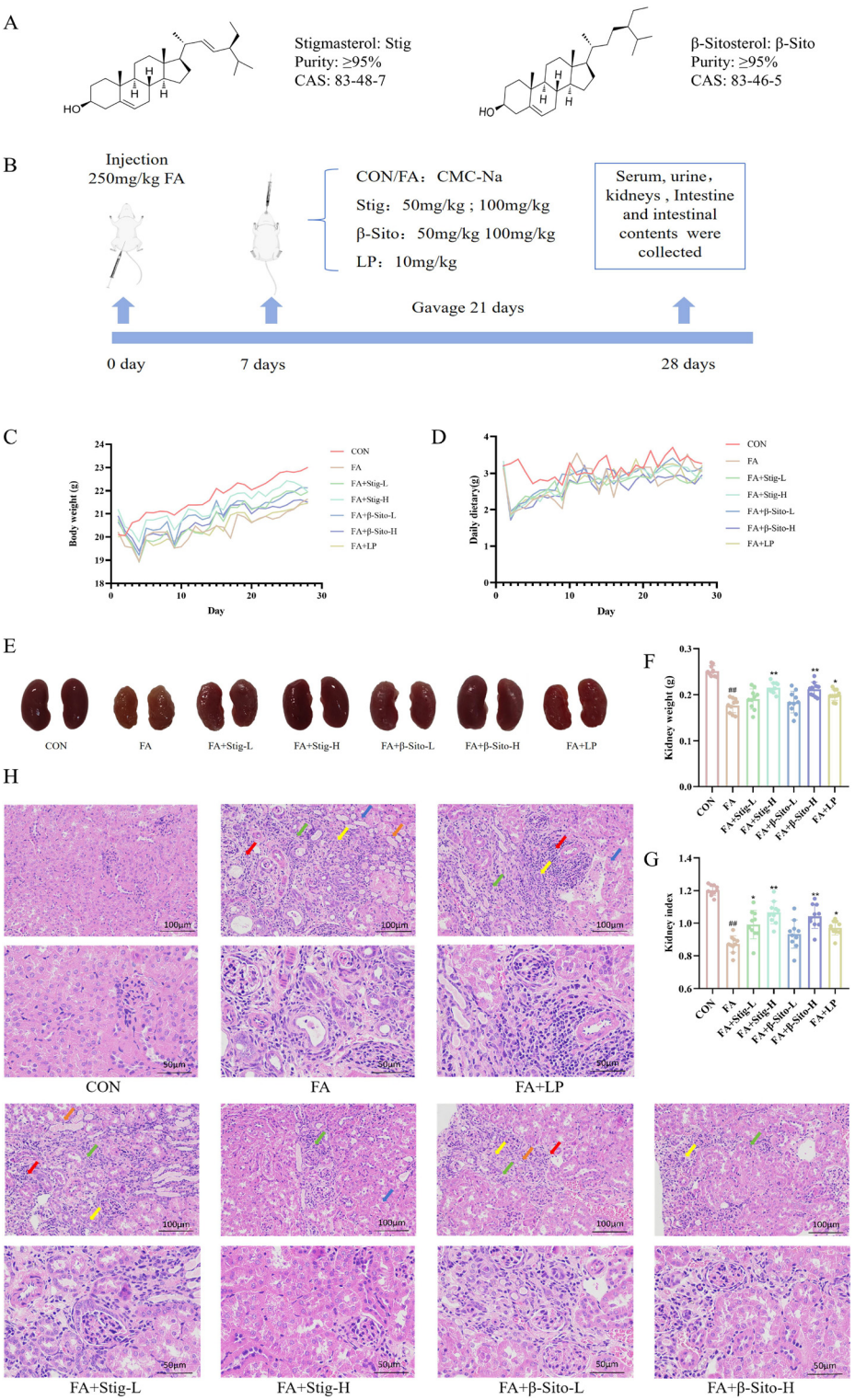

Fig. 1 (A) Chemical structures of stigmasterol and β-sitosterol. (B) Schematic diagram of the animal experiment. (C) Body weight. (D) Daily dietary. (E) Morphological images of kidney tissue. (F) Kidney weight. (G) Kidney index. (H) HE staining of kidney tissue. $^{\#\#}P < 0.01$ FA *vs.* CON; $^{*}P < 0.05$; FA + Stig-L/H, FA + LP *vs.* FA; $^{**}P < 0.01$ FA + Stig-H, FA + β-Sito-H *vs.* FA. Data are shown as mean ± SD. ((F and G) $n = 10$), ((H) $n = 3$).

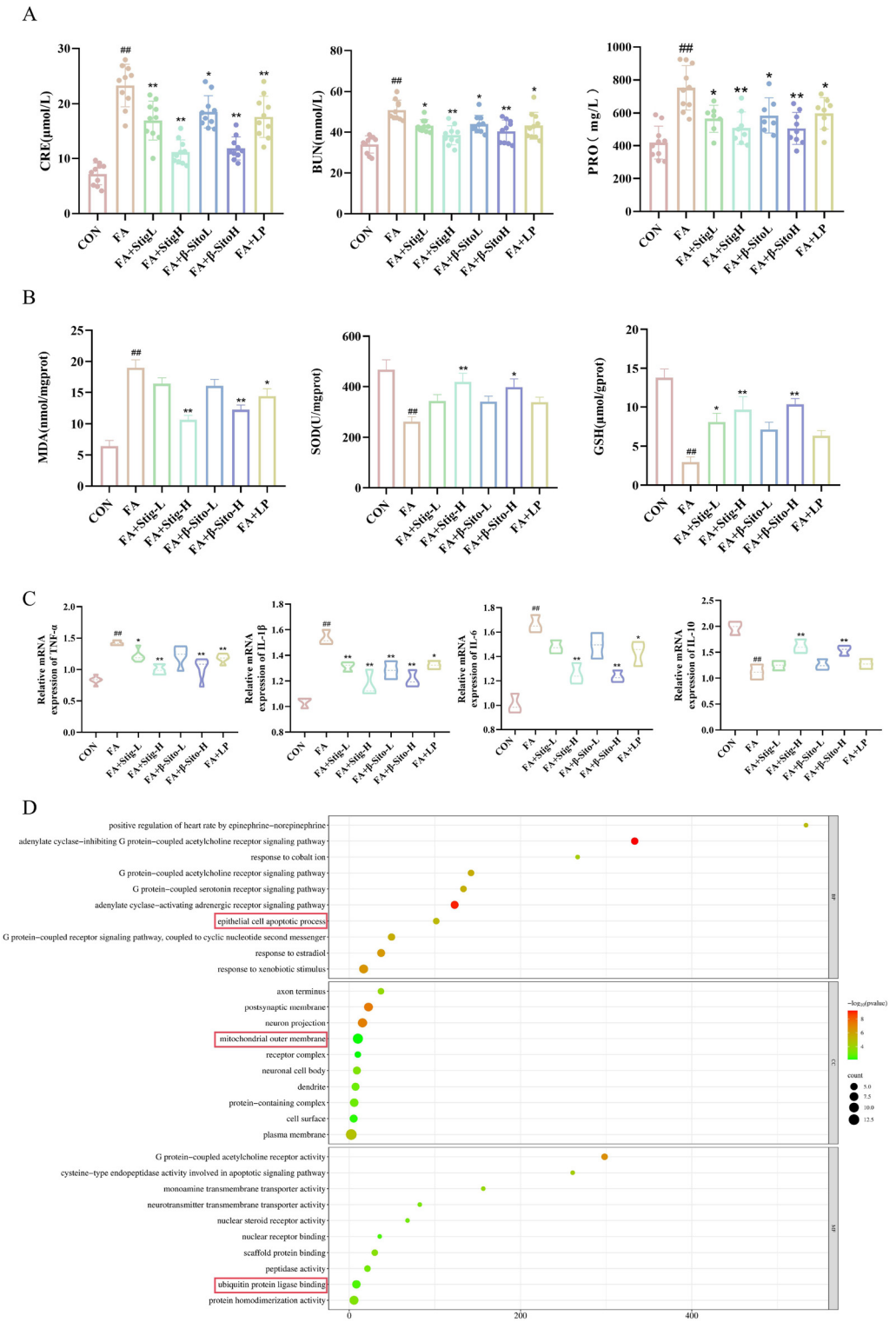

Fig. 2 (A) CER, BUN and PRO levels. (B) Content of MDA, SOD, and GSH in kidney tissue supernatants. (C) mRNA expression levels of TNF-α, IL-1β, IL-6, and IL-10 in kidney tissue. (D) GO enrichment analysis of PS-related genes. $^{\#\#}P < 0.01$ FA *vs.* CON; $^{*}P < 0.05$; FA + Stig-L, FA + β-Sito-L/H, FA + LP *vs.* FA; $^{**}P < 0.01$ FA + Stig-H, FA + β-Sito-H, FA + LP *vs.* FA. Data are shown as mean ± SD. ((A and B) $n = 10$), ((C) $n = 6$).

renal function by regulating oxidative stress and inflammatory factors.

GO enrichment analysis of PS-related genes revealed that PS may play a crucial role in several biological processes and molecular functions, including the adenylate cyclase inhibition of G protein-coupled acetylcholine receptor signaling pathways, epithelial cell apoptosis, mitochondrial outer membrane, and ubiquitin protein ligase binding (Fig. 2D).

3.3 PS reduced renal fibrosis in CKD mice by inhibiting the TGF-β/Smad pathway

Continuous oxidative stress and inflammatory responses during CKD progression can lead to renal fibrosis, which gradually destroys normal kidney structure and function.[35,36] The extent of fibrosis is directly correlated with renal function decline. Masson staining was used to assess fibrosis in kidney tissues from all groups. Results demonstrated that the FA group had a higher degree of fibrosis, with more collagen fiber deposition and a larger fibrosis area than the CON group (Fig. 3A). Protein expression of α-smooth muscle actin (α-SMA), collagen type I (COL-1), and fibronectin (FN1) was significantly elevated in the FA group. In comparison with the FA group, the Stig-H, β-Sito-H, and LP groups exhibited a significant reduction in collagen deposition, fibrosis area, and the expression of fibrosis-related proteins, as illustrated in Fig. 3B and C. These findings are consistent with the results obtained from RT-qPCR analysis (Fig. 3D). The TGF-β/Smad signaling pathway plays a key role in fibrosis development, and renal tubulointerstitial fibrosis is directly related to its dysregulation.[3–5] We analyzed TGF-β/Smad pathway mRNA and protein expression, finding increased renal TGF-β, p-Smad2/Smad2, and p-Smad3/Smad3 levels in the FA group, alongside decreased Smad7 expression. The PS treatment resulted in a significant, concentration-dependent reduction in the levels of TGF-β, p-Smad2/Smad2, and p-Smad3/Smad3, while concurrently enhancing the expression of Smad7 mRNA and protein. In contrast, the LP group did not demonstrate a statistically significant effect on the protein expression levels of TGF-β, Smad3, and Smad7 (Fig. 4A–D). These results suggest that PS mitigate renal fibrosis by blocking the TGF-β/Smad signaling pathway and reducing fibrosis-associated protein production.

3.4 Transmission electron microscopy and transcriptome sequencing result analysis

Organelle damage in CKD is influenced by multiple factors, leading to cell dysfunction and death, which ultimately exacerbates kidney pathology and accelerates CKD progression.[37,38] Therefore, targeting organelle function is considered a viable therapeutic approach for CKD. Kidney tissues from each group were examined *via* TEM. Compared with the CON group, proximal tubular epithelial cells in the FA group exhibited moderate edema and partial dissolution of the cell membrane. There was a significant reduction in the number of organelles, most of which displayed swelling. The number of mitochondria (M) decreased, and they showed signs of damage and disintegration, with shortened or absent cristae. The rough endoplasmic reticulum (RER) was reduced in number, significantly expanded, and showed membrane damage, with a few ribosomes visible on its surface. Intramembrane folds of the plasma membrane disappeared, and lipid droplets (LD) of uneven size were observed and fused. Autophagic lysosome structures (ASS) were also visible. After PS intervention, cell swelling, the number of organelles, and mitochondrial quantity and morphology were restored, and autophagic lysosome structures disappeared (Fig. 5A).

To further investigate the mechanisms by which PS mitigate CKD, RNA sequencing (RNA-seq) was performed on kidney tissues from the CON, FA, Stig, and β-Sito groups. The findings revealed that 138 genes were downregulated and 608 genes were upregulated in the FA group compared to the CON group. In contrast, the Stig group had 301 downregulated and 144 upregulated genes compared to the FA group, while the β-Sito group exhibited 292 downregulated and 204 upregulated genes. The intersection of upregulated genes from the FA group and downregulated genes from the PS groups revealed 122 common genes, which may be related to the remission of CKD by PS (Fig. 5B and C). The top 10 differentially expressed genes, based on *p*-values, were used for heatmap analysis. Notably, Sting1 levels in the PS groups tended to normalize, approaching those observed in the CON group (Fig. 5D). Sting1 was entered into the KEGG database to retrieve its upstream and downstream genes, allowing for further investigation of the cGAS/Sting1/TBK1 signaling pathway.

KEGG enrichment analysis showed that the pathways involved in the alleviation of CKD by PS included cytokine–cytokine receptor interaction, phagosome, and EC–receptor interaction (Fig. 5E). Using "mitophagy" as the keyword, a total of 5171 related genes were retrieved in GeneCards. Based on correlation scores, the top 10 genes were selected for transcriptomic heatmap analysis. The data analysis results of GeneCards show that PINK1 and Parkin had high correlation scores with mitophagy (Fig. 5G). The transcriptome analysis showed that PINK1 and Parkin were increased after PS intervention (Fig. 5F). Consequently, the PINK1/Parkin-mediated mitophagy pathway was chosen for further investigation.

3.5 PS inhibited the cGAS/Sting1/TBK1 pathway

Western blot results demonstrated that the expression levels of cGAS, Sting1, and TBK1 proteins were significantly higher in the FA group compared to the CON group. Following Stig and β-Sito administration, there was a reduction in cGAS, Sting1, and TBK1 expression levels (Fig. 6A and B). RT-qPCR results confirmed that the mRNA expression levels of the major genes aligned with the western blot data (Fig. 6C).

3.6 PS promoted the PINK1/Parkin-mediated mitophagy pathway

Protein expression levels related to mitophagy are shown in Fig. 7A and B. The FA group exhibited higher levels of PINK1, Parkin, and LC3 protein expression compared to the CON

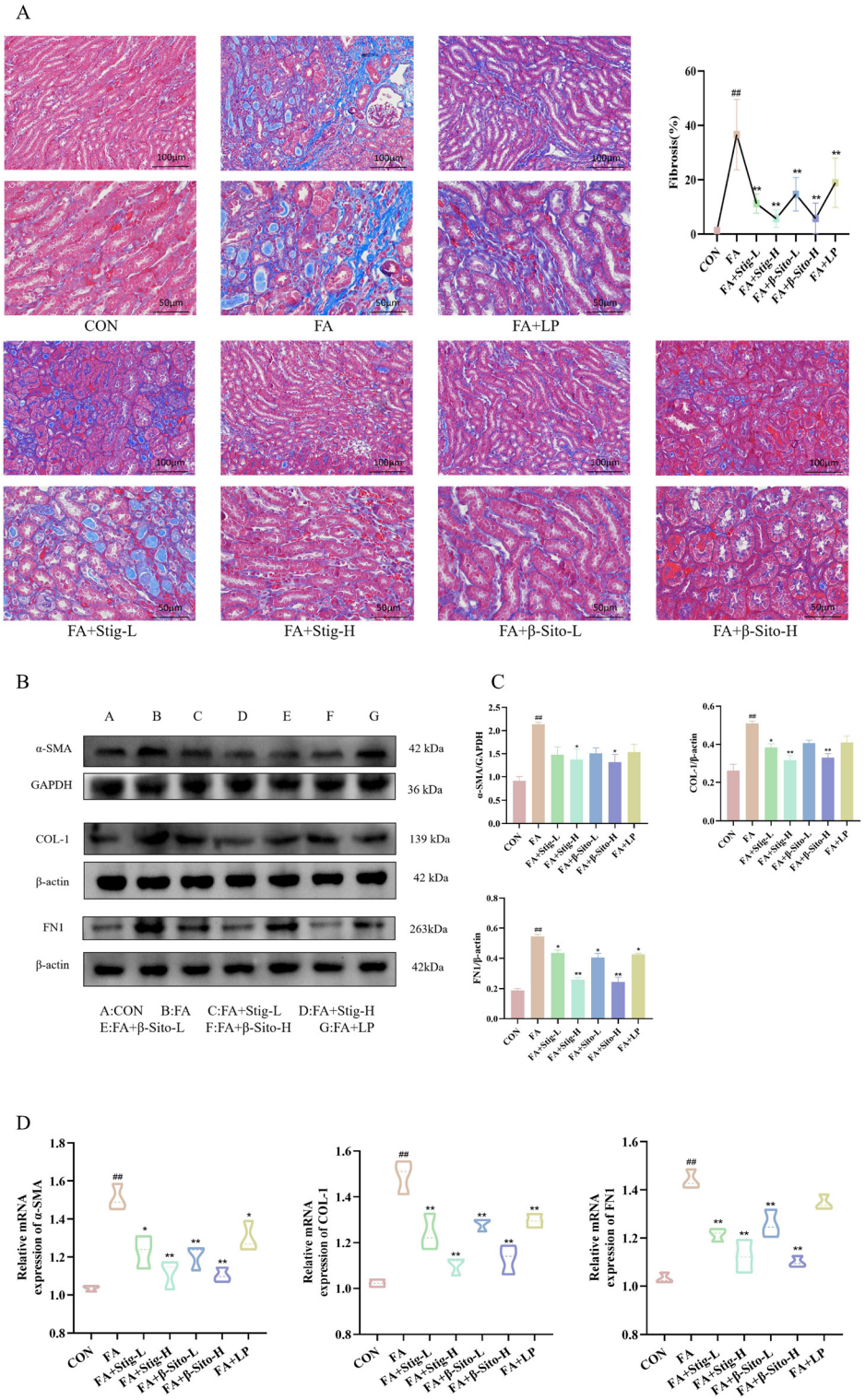

Fig. 3 (A) Masson staining. (B–C) α-SMA, COL-1, and FN1 protein expression levels. (D) mRNA expression levels of α-SMA, COL-1, and FN1. $^{\#\#}P < 0.01$ FA *vs.* CON; $^{*}P < 0.05$; FA + StigL/H, FA + β-SitoL/H, FA + LP *vs.* FA; $^{**}P < 0.01$ FA + StigL/H, FA + β-SitoL/H, FA + LP *vs.* FA. Data are shown as mean ± SD. ((A–C) $n = 3$), ((D) $n = 6$).

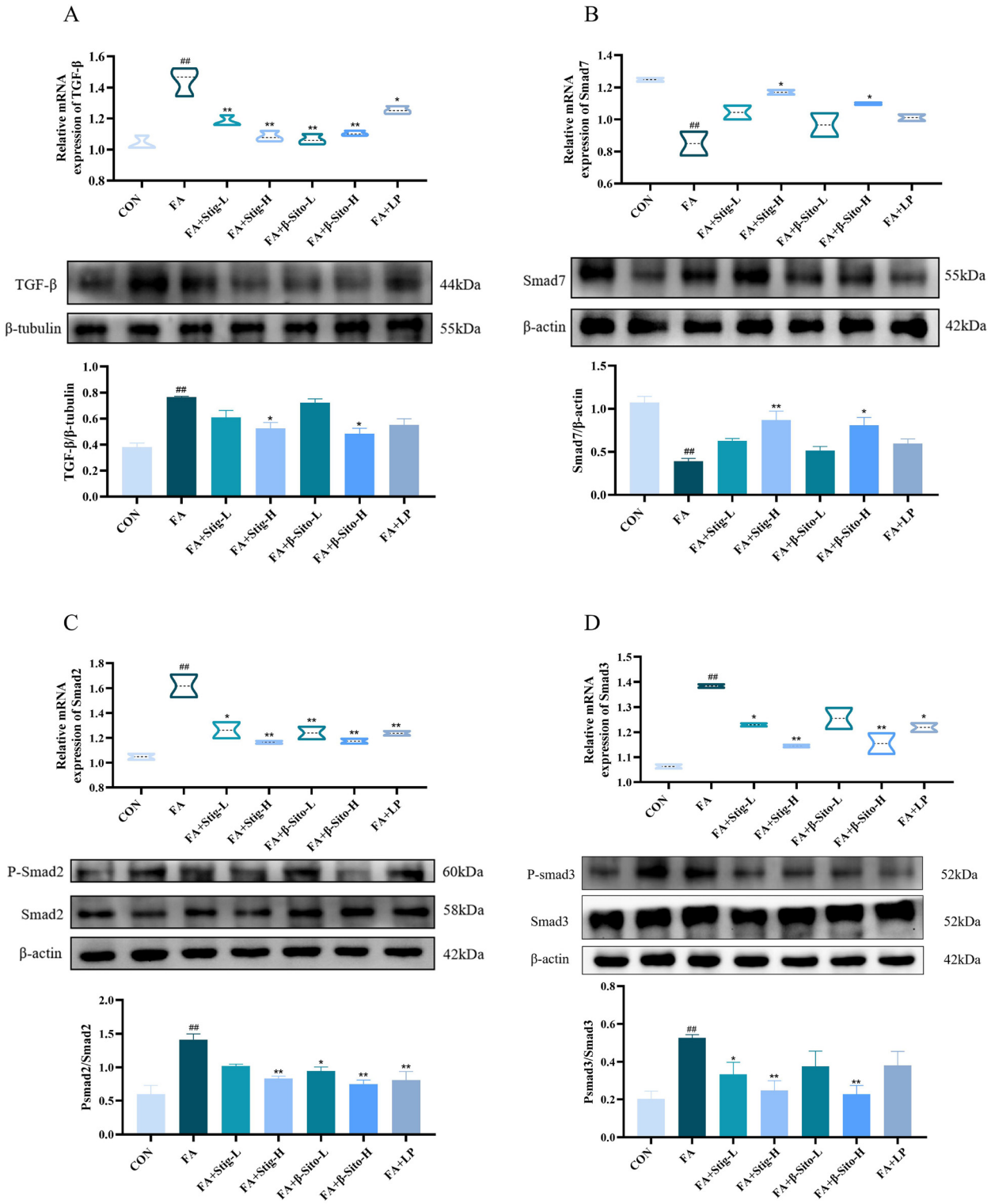

Fig. 4 (A) mRNA and protein expression levels of TGF-β. (B) mRNA and protein expression levels of Smad7. (C) mRNA and protein expression levels of Smad2. (D) mRNA and protein expression levels of Smad3. ($^{\#\#}P < 0.01$ FA *vs.* CON; $^{*}P < 0.05$; FA + StigL/H, FA + β-SitoL/H, FA + LP *vs.* FA; $^{**}P < 0.01$ FA + StigL/H, FA + β-SitoL/H, FA + LP *vs.* FA). Data are shown as mean ± SD. (Data of RT-qPCR $n = 6$; data of western blot $n = 3$).

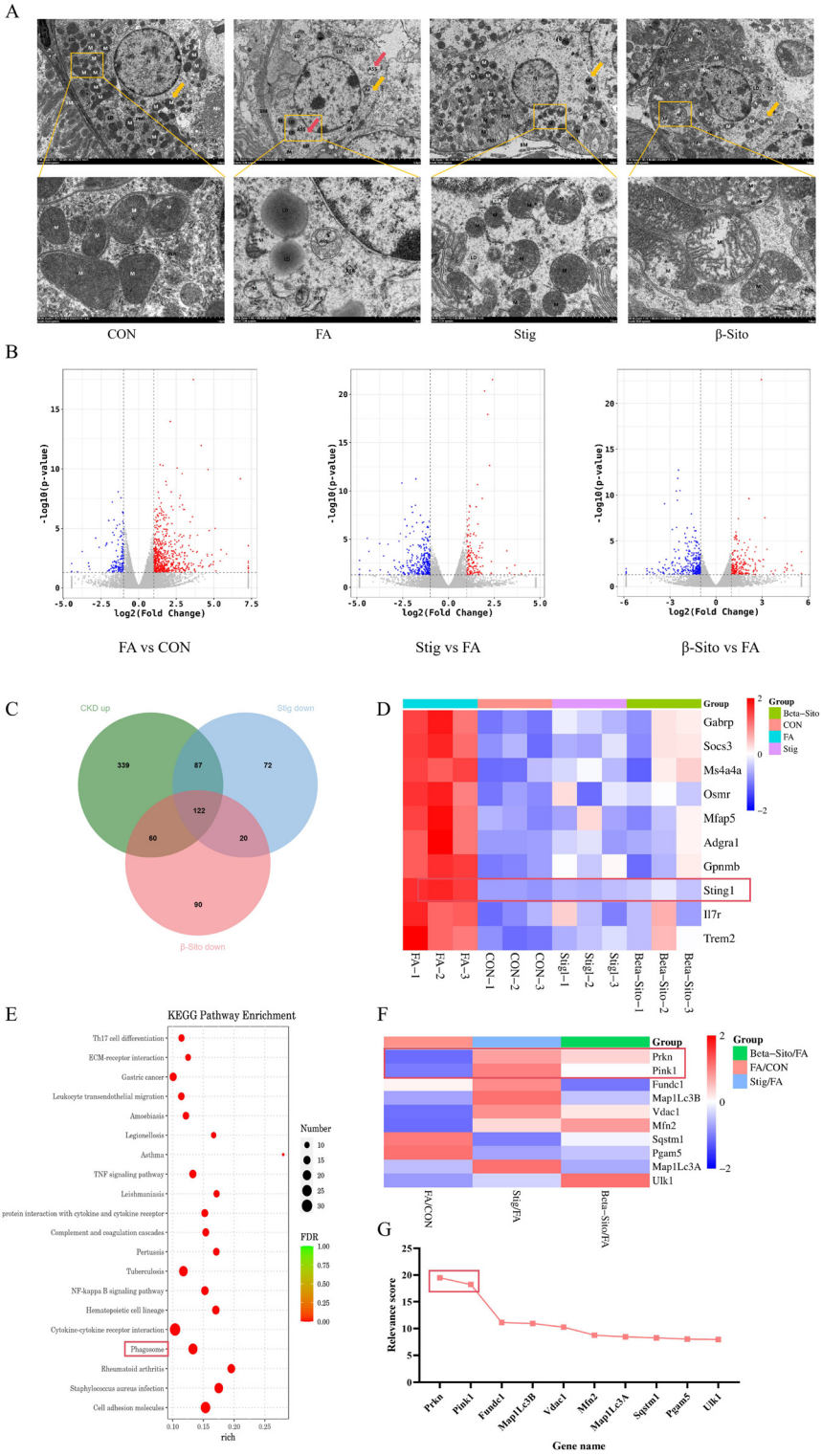

Fig. 5 (A) Transmission electron microscopy results of kidney tissue. (B) Volcano plot of gene changes. (C) Venn diagram of differentially expressed genes. (D) Heat map analysis of genes in CKD mice treated with PS. (E) KEGG pathway enrichment analysis. (F) Heatmap analysis of mitophagy-related genes. (G) Correlation scores of mitophagy genes.

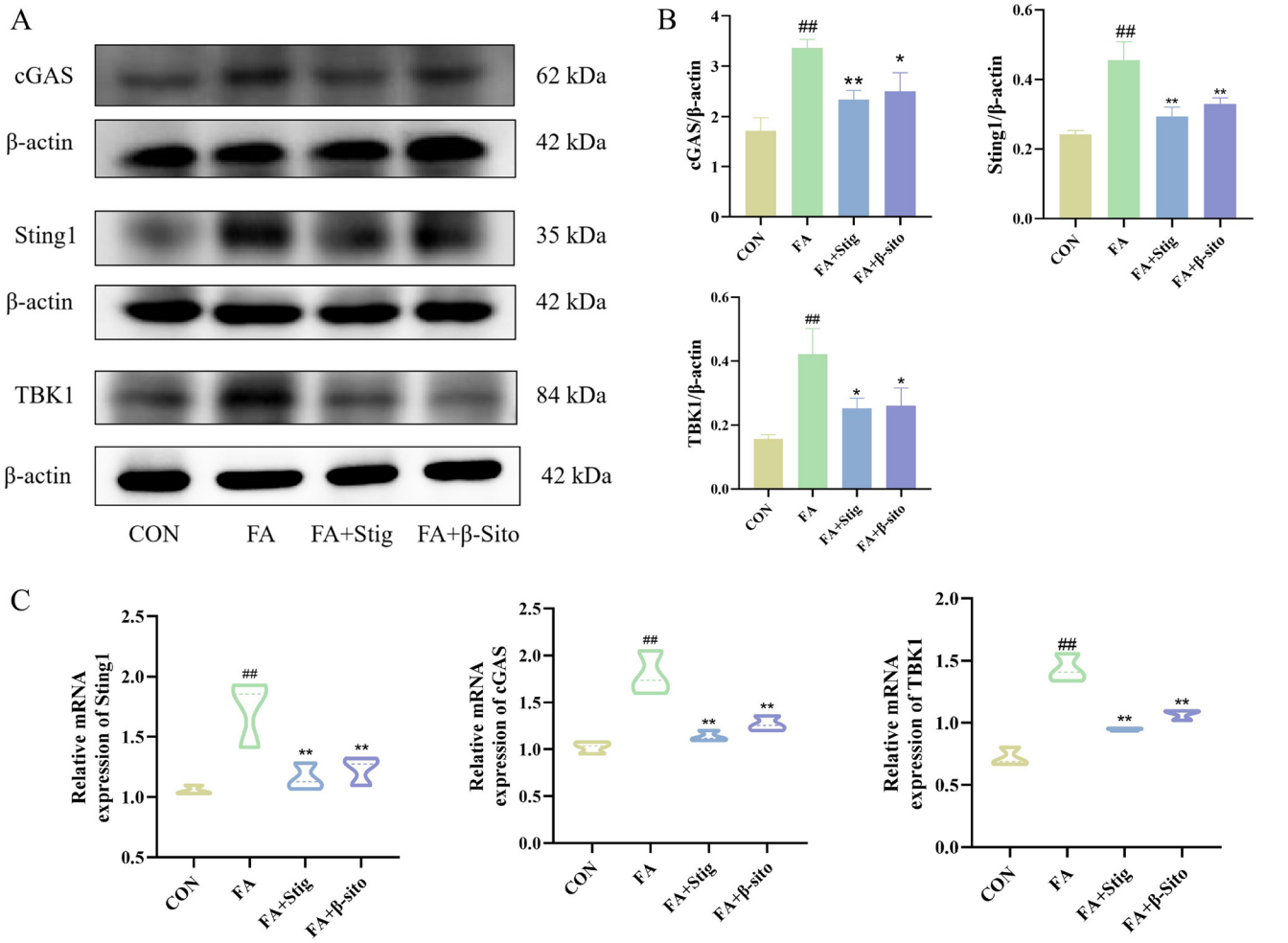

Fig. 6 (A and B) Protein expression levels of the cGAS/Sting1/TBK1 pathway. (C) mRNA expression levels of the cGAS/Sting1/TBK1 pathway. ($^{\#\#}P < 0.01$ FA *vs.* CON; $^{*}P < 0.05$; FA + Stig, FA + β-Sito *vs.* FA; $^{**}P < 0.01$ FA + Stig, FA + β-Sito *vs.* FA). Data are shown as mean ± SD. ((A and B) $n = 3$; (C) $n = 6$).

group, while P62 expression levels were significantly reduced. In contrast, PS intervention resulted in increased PINK1, Parkin, and LC3 protein expression, along with a substantial decrease in P62 levels, relative to the FA group. RT-qPCR results confirmed that the mRNA expression levels of the relevant genes were consistent with the western blot findings (Fig. 7C).

3.7 PS regulated the intestinal barrier and the composition of the gut microbiota of CKD mice

The gut microbiota can enhance the intestinal barrier and regulate intestinal inflammation. Maintaining intestinal barrier integrity and healthy gut flora may be key strategies for CKD prevention and therapy.[39] HE staining of the small intestine showed that, compared to the CON group, the FA group exhibited disorganized villi structures, with frequent detachment of villi and epithelial cells, exposing the lamina propria. The villi structures were unclear, and the intestinal gland structures were indistinct. A reduction in the number of intestinal glands within the lamina propria was also observed, with a sparse arrangement of glands and increased spacing between them. After PS intervention, these pathological conditions of the small intestine improved (Fig. 8A).

Owing to the increased dosage of the PS intervention, there was an enhanced remission effect on CKD. Consequently, gut microbiota detection and analysis were performed on the CON, FA, Stig, and β-Sito groups. Using 16S rDNA gene sequencing, the gut microbiota composition of mice following PS intervention was analyzed. The Venn diagram showed the number of ASVs (amplicon sequence variants) shared and unique to each group, with 538 common ASVs identified across the four groups. Unique ASVs included 125 in the CON group, 318 in the FA group, 243 in the Stig group, and 245 in the β-Sito group (Fig. 8B). Bray–Curtis PCoA analysis revealed that the samples from the CON group clustered closely, indicating smaller within-group variance. There was some degree of separation between the FA and CON groups, while after the PS intervention, the Stig group gravitated toward the CON group (Fig. 8C). The Shannon curve indicated that the sequencing data were sufficient to

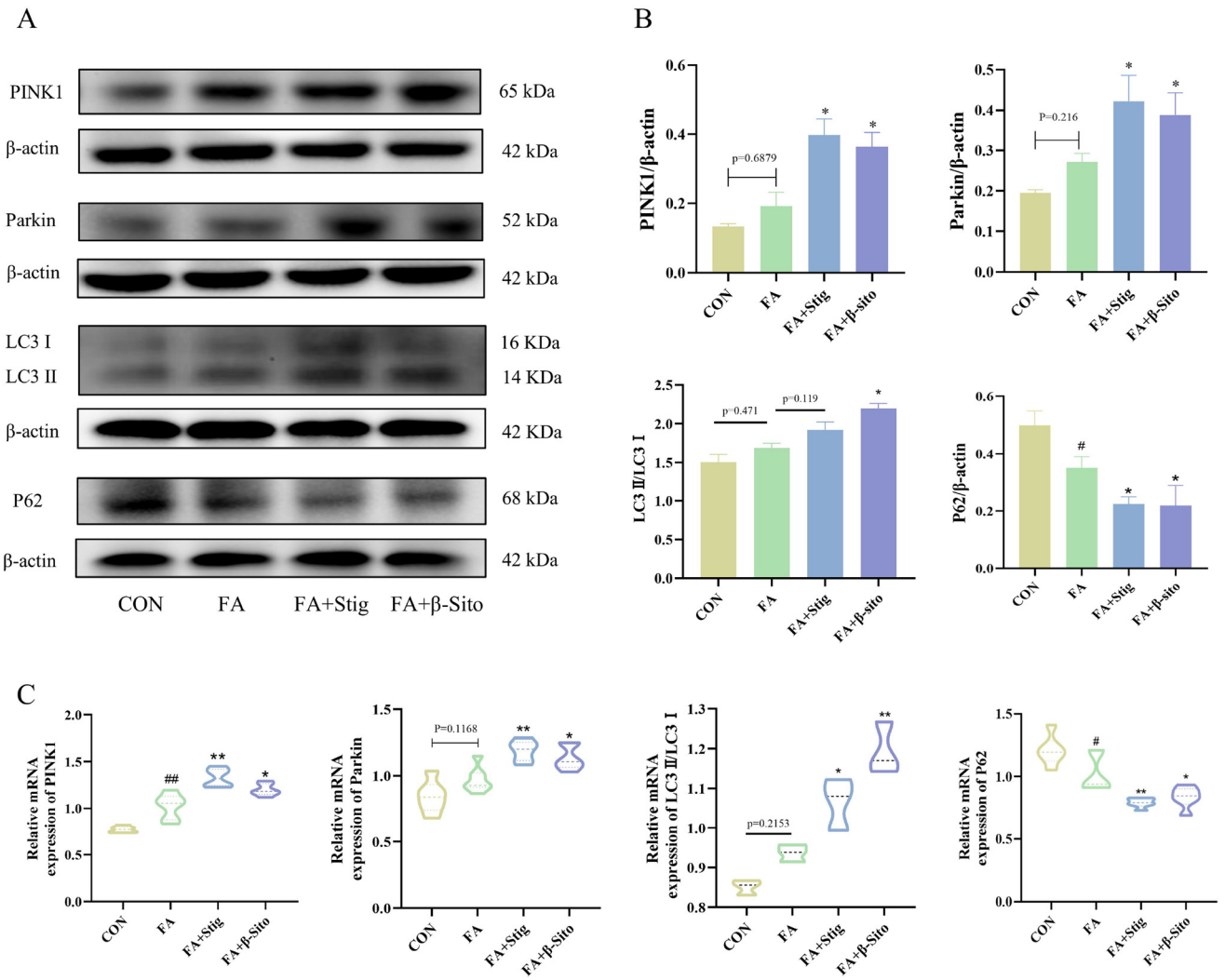

Fig. 7 (A and B) Protein expression levels of PINK1, Parkin, LC3, P62. (C) mRNA expression levels ofPINK1, Parkin, LC3, P62. ($^{\#}P < 0.05$ FA *vs.* CON; $^{*}P < 0.05$; FA + Stig, FA + β-Sito *vs.* FA; $^{**}P < 0.01$; FA + Stig *vs.* FA). Data are shown as mean ± SD. ((A and B), $n = 3$; (C), $n = 6$).

capture the majority of microbiological information (Fig. 8D), and the abundance curve suggested that the species distribution within samples was relatively even (Fig. 8E). The Chao index, reflecting species richness, showed a significant increase in species quantity after FA injection compared to the CON group, with a decreasing trend observed after PS intervention (Fig. 8F). The Shannon index, reflecting species diversity, showed that FA injection significantly increased gut microbiota diversity, while the Stig group exhibited a significant reduction in diversity (Fig. 8G). The Simpson index indicated that species distribution across groups was relatively even (Fig. 8H).

The microbial composition was determined at various taxonomic levels, including kingdom, phylum, class, order, family, genus, and species. At the phylum level, *Firmicutes* and *Bacteroidota* were the dominant microbiota (Fig. 9A). Significant differences in the microbial composition were observed across groups at the genus and species levels, while the microorganisms at the species level were all undefined flora. Thus, the analysis focused on genus-level differences (Fig. 9B). Probiotic genera, such as *Muribaculaceae* and *Alloprevotella*, decreased significantly in the FA group but increased after PS intervention. Pathogenic genera, such as *Alistipes* and *Odoribacter*, increased markedly in the FA group but decreased significantly after PS intervention (Fig. 9C and D). To further assess differences between groups, LEfSe (Linear discriminant analysis Effect Size) analysis was performed. The results indicated that in the CON group, 8 types of bacteria, including *Burkholderiales* and *Gammaproteobacteria*, played important roles. In the FA group, 12 types of bacteria, including *Rikenellaceae* and *Veillonellaceae*, were significant. In the Stig group, 3 types of bacteria, including *Lactobacillaceae* and *Oscillospirales*, were important, while in the β-Sito group, 7 types of bacteria, including *Acholeplasmataceae* and *Mycoplasmataceae*, were identified as significant (Fig. 9E and F).

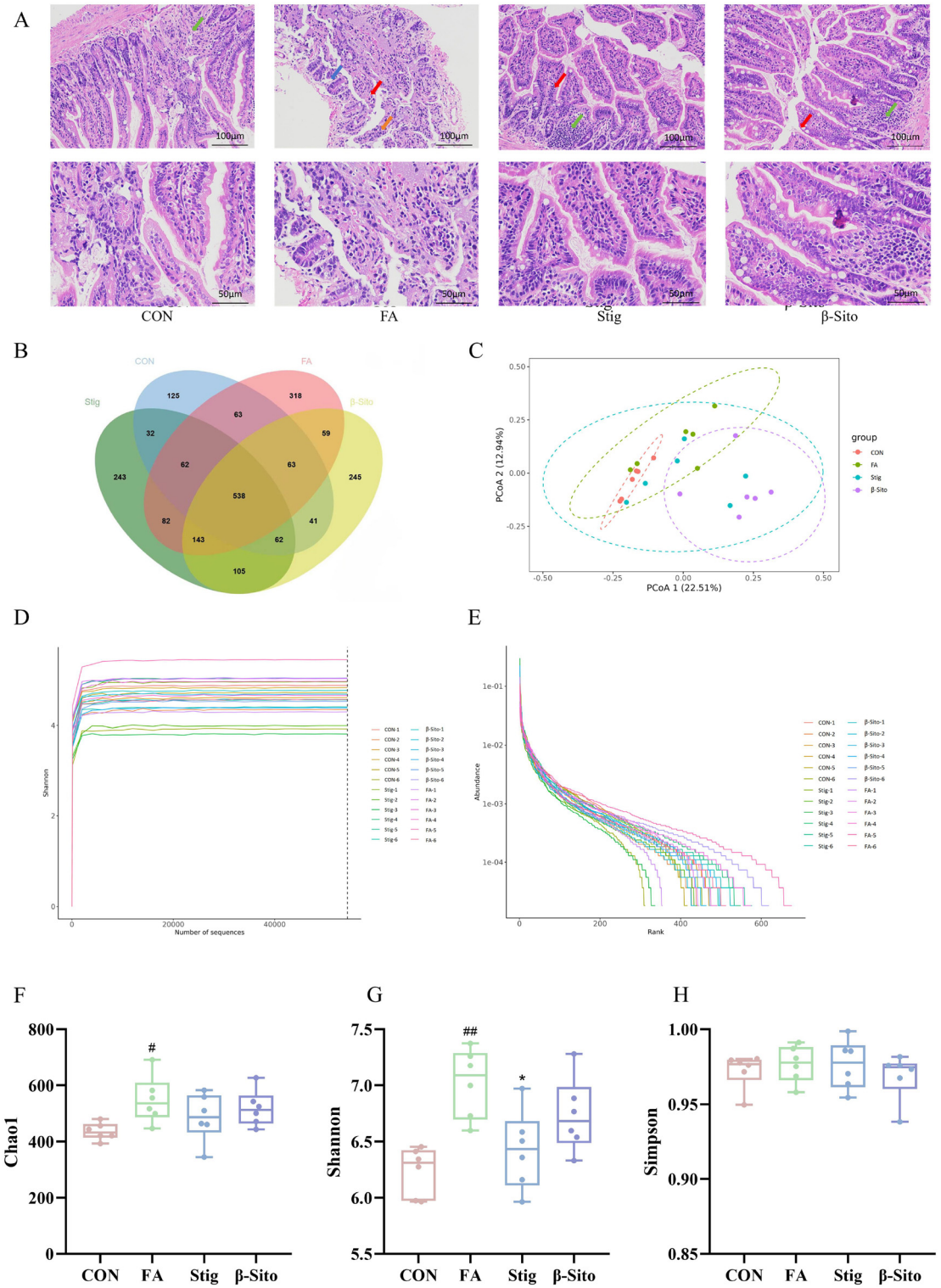

Fig. 8 (A) HE staining results of the small intestine. (B) Venn diagram of ASV intersection. (C) PCoA analysis. (D) Shannon curve. (E) Abundance curve. (F) Chao1 index. (G) Shannon index. (H) Simpson index. ($^{\#}P < 0.05$ FA *vs.* CON; $^{\#\#}P < 0.01$ FA *vs.* CON; $^{*}P < 0.05$; FA + Stig *vs.* FA). data are shown as mean ± SD. ($n = 6$).

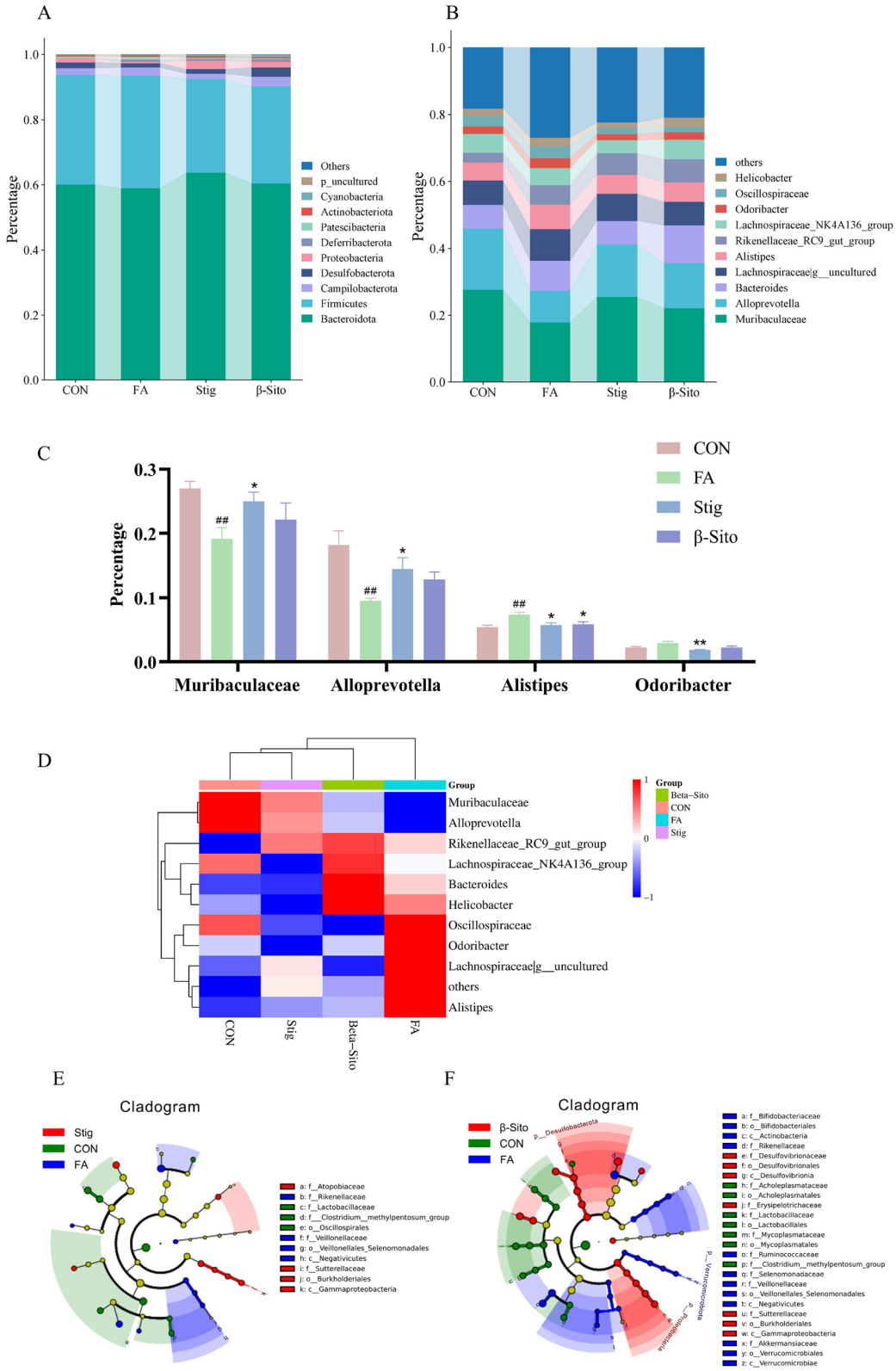

Fig. 9 (A) Microbial distribution at the phylum level. (B) Microbial distribution at the genus level. (C) Percentage analysis of microbes at the genus level. (D) Heat map analysis of microbes at the genus level. (E) and (F) LEfSe analysis. Data are shown as mean ± SD. (n = 6).

4. Discussion

This study investigated the potential efficacy of two phytosterols, stigmasterol and β-sitosterol, in ameliorating CKD. The findings present compelling evidence that the PS influence pathological alterations in renal tissues and exert effects on CKD by regulating multiple pathophysiological mechanisms, including oxidative stress, inflammation, renal fibrosis, mitophagy, and gut microbiota modulation. Firstly, it was demonstrated that PS could decrease the concentrations of MDA and pro-inflammatory mediators, including IL-6, IL-1β, and TNF-α. Additionally, PS were shown to enhance the levels of SOD, GSH, and the anti-inflammatory IL-10. Another significant finding is PS's ability to mitigate renal fibrosis, a predominant driver of CKD progression. The TGF-β signaling pathway is critically involved in the EMT process, which promotes fibrosis. Activation of this pathway by increasing the phosphorylation of Smad2 and Smad3 and reducing Smad7 levels transactivates downstream profibrotic proteins, thereby promoting fibrosis development.[40,41] This study demonstrated that the Stig-H and β-Sito-H groups more effectively inhibited the expression of fibrosis marker proteins, including α-SMA, COL-1, and FN1, as well as TGF-β, p-Smad2, and p-Smad3 proteins, while simultaneously enhancing Smad7 expression, compared to the LP group. These findings suggest that PS attenuates FA-induced fibrosis in mice by modulating the TGF-β/Smad signaling pathway, highlighting its potential as a novel strategy for the mitigation of CKD .

To further explore how PS alleviate CKD, a bioinformatic analysis of transcriptomic data was conducted, followed by experimental validation. Transcriptomic analysis identified 122 differentially expressed genes (DEGs) that were upregulated in the FA group but downregulated in the PS groups. Among these, Sting1 exhibited significant changes in both PS groups. KEGG pathway analysis suggested that PS mitigation of CKD may involve the phagocytosis pathway. Therefore, Sting1 and its upstream and downstream genes were selected for further investigation of the cGAS/Sting1/TBK1 signaling pathway, a major sensor of inflammation induced by mitochondrial DNA (mtDNA) release.[42–44]

Mitophagy, the selective degradation of defective mitochondria through autophagic processes, is crucial for maintaining mitochondrial quality control, which helps prevent mtDNA release and restrict activation of the cGAS/Sting1/TBK1 axis.[45,46] PINK1 and Parkin are key mediators of this process.[47] Consequently, the PINK1/Parkin-mediated mitophagy pathway was selected for further analysis. RT-qPCR and western blot confirmed that PS downregulated the expression of cGAS, Sting1, and TBK1, while activating PINK1/Parkin-mediated mitophagy. These findings suggest that PS attenuate renal fibrosis by inhibiting the cGAS/Sting1/TBK1 inflammatory pathway and activating mitophagy.[48,49]

The gut microbiota has recently gained attention as a potential contributor to the pathogenesis of kidney diseases.[50] The "gut–kidney axis" highlights the connection between CKD and the gut microbiota.[51] Dysbiosis and reduced diversity in the gut microbiome are strongly associated with CKD. Gut bacteria contribute to renal disease progression by modulating intestinal barrier function and promoting chronic inflammation through biochemical toxins.[11,14] Functional ingredients and nutrients such as fiber, probiotics, synbiotics, and phytoconstituents can modulate inflammatory pathways or influence the gut mucosa, potentially decelerating CKD progression.[52]

Previous research has established that the intestine serves as the primary site for phytosterol absorption. Phytosterols have been shown to alter the villus length and crypt depth in the small intestines of osteoporotic mice, and they can modify intestinal morphology through the regulation of the intestinal microbiota, which suggests the potential role of phytosterols in mitigating osteoporosis through their interaction with the gut microbiota.[53] These findings are consistent with the results of our study, which shows that PS improve intestinal permeability by mitigating villi structural abnormalities, reducing frequent detachment of villi and epithelial cells, and minimizing lamina propria exposure in the kidneys and small intestines. Furthermore, PS also increase the number and reduce the spacing of intestinal glands in the lamina propria. In brief, PS regulate the intestinal barrier and gut microbiota composition in CKD mice.

Furthermore, 16S rDNA gene sequencing results revealed that PS attenuate the enhanced species diversity of the gut microbiota in CKD mice. PS significantly elevated the abundance of probiotics such as *Muribaculaceae* and *Alloprevotella*, while notably decreasing pathogenic genera like *Alistipes* and *Odoribacter*. Research studies indicated that *Alloprevotella* and *Muribaculaceae* aid in the production of short-chain fatty acids (SCFAs) in the intestines, which may enhance intestinal epithelial cell growth, restore the intestinal epithelial barrier integrity, and prevent intestinal endotoxin leakage into the bloodstream. These probiotics protect intestinal barrier function and exert direct and indirect anti-inflammatory effects.[54,55] However, *Odoribacter* and *Alistipes*, pro-inflammatory bacteria linked to various inflammatory diseases, can activate inflammatory signaling pathways, leading to increased pro-inflammatory factors and reduced anti-inflammatory factors. These bacterial species are strongly associated with kidney injury, suggesting they may play an essential role in PS's mitigation mechanism for CKD.[56,57] Thus, altering the gut microbiota through PS supplementation may be a promising strategy for CKD remission.

This research explored the physiological mechanism of PS's anti-fibrotic effects in CKD mice. Based on the aforementioned research findings, it can be concluded that there were no significant differences between the two high-dose treatments of stigmasterol and β-sitosterol concerning kidney tissue pathology, the extent of fibrous reduction, recovery of kidney function indicators, and the regulation of oxidative stress and inflammatory factors. High-dose PS exhibited superior effects compared to low-dose PS and LP. In terms of inhibiting the cGAS/Sting1/TBK1 pathway and modulating the gut microbiota, stigmasterol demonstrated more effective intervention outcomes than β-sitosterol. Despite substantial experimental evidence, the study has limitations. The roles of *Odoribacter*,

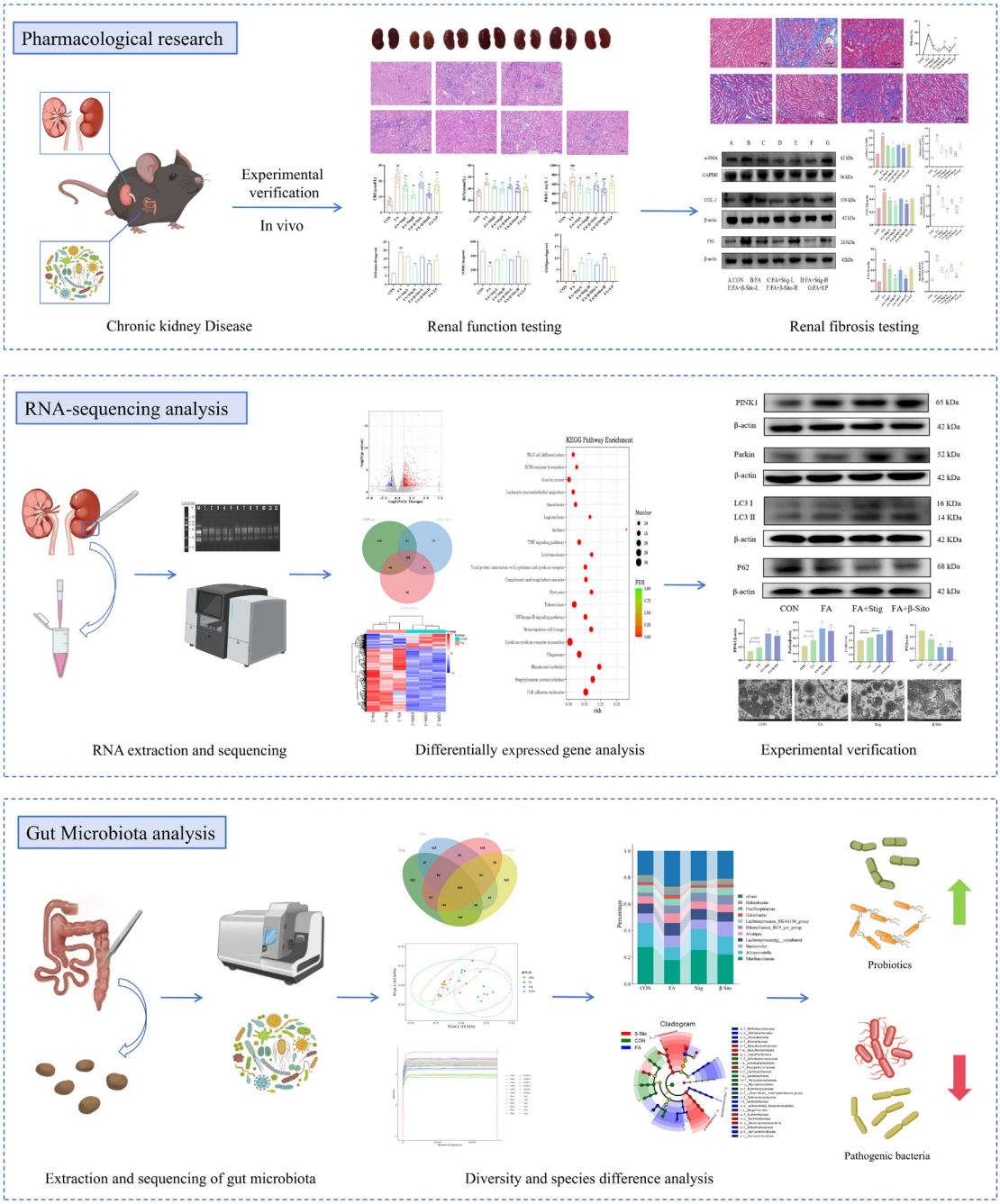

Fig. 10 Possible mechanisms for the phytosterols alleviating CKD.

Alistipes, *Alloprevotella*, and *Muribaculaceae* in renal damage have not been fully investigated. Future research should focus on clarifying the pathophysiology and evolution of the gut microbiota in CKD, including changes in metabolite profiles.

5. Conclusion

In this study, we investigated the effects of PS, especially stigmasterol and β-sitosterol, on alleviating symptoms in CKD mice and explored the underlying mechanisms. PS mitigated renal damage by inhibiting inflammation and fibrosis, primarily through activating PINK1/Parkin-mediated mitophagy and suppressing inflammation *via* the cGAS/Sting1/TBK1 signaling pathway. Moreover, PS demonstrated the potential to improve intestinal permeability. Experimental evidence suggests that the intestinal microbiota significantly mediates PS's alleviation effects. These findings offer fresh insights into the gut–kidney axis and enhance the understanding of PS's mitigation potential in CKD. These findings propose PS as a promising candi-

date for therapeutic intervention, potentially suitable for dietary supplementation, and are anticipated to offer a theoretical foundation for the effective application of PS supplementation in the management of CKD (Fig. 10).

Ethics statement

The care and use of the laboratory animals were conducted according to the guidelines of the International Council for Laboratory Animal Science. All experimental protocols were reviewed and approved by the Ethics Committee of the China Institute for Radiation Protection, Taiyuan, China (License No. CIRP-IACLLC-(R)2024020).

Author contributions

XiuE Feng: conceptualization, project administration, and funding acquisition. Jiangtao Zhou: methodology, supervision, and writing – review & editing. Fan Yang: conceptualization, project administration, resources, writing – original draft, and writing – review & editing. Yingjie Gao: validation, visualization, software, writing – original draft, and writing – review & editing. Siyi Xie: validation and writing – review & editing. Wenjing Yang: investigation and writing – review & editing. Qiyan Wang: investigation and writing – review & editing. Wenqian Ye: software and writing – review & editing. Lu Sun: data curation.

Data availability

Data will be made available on request.

Conflicts of interest

The authors declare that they have no known competing financial interests or personal relationships that could have appeared to influence the work reported in this paper.

Acknowledgements

This work was financially supported by the Shanxi Fundamental Research Program (No. 202303021221129), the special Fund from Medicinal Basic Research Innovation Center of Chronic Kidney Disease, Ministry of Education, Shanxi Medical University (No. CKD/SXMU-2024–10), the Shanxi Medical University Technology Leading Special Project (BYJL026), and The Open Fund of Shanxi Key Laboratory of Innovative Drugs for the Treatment of Serious Diseases Based on Chronic Inflammation, Shanxi University of Chinese Medicine (SXInFDL2024–0010). The authors acknowledge the assistance of the postdoctoral workstation, the fifth Hospital of Shanxi Medical University (Shanxi Provincial People's Hospital), Taiyuan, China and Medicinal Basic Research Innovation Center of Chronic Kidney Disease, the Ministry of Education, Shanxi Medical University, and the funding from the National Natural Science Foundation of China and Shanxi Fundamental Research Program.

References

1 C.-L. Chou, H.-W. Chiu, Y.-H. Hsu, S. M.-W. Yu, T.-H. Liou and L.-C. Sung, Impact of chronic kidney disease and end-stage renal disease on the mid-term adverse outcomes in diabetic patients with cardiovascular diseases, *Sci. Rep.*, 2024, **14**, 1–11.
2 Y. Liu, J. Wu, S. Liang, J. Xu, M. Wei, Z. Du and S. Qiang, Guben Xiezhuo Decoction inhibits M1 polarization through the Raf1/p-Elk1 signaling axis to attenuate renal interstitial fibrosis, *J. Ethnopharmacol.*, 2024, **319**, 117189.
3 Y. Wang, Z. Ping, H. Gao, Z. Liu, Q. Xv, X. Jiang and W. Yu, LYC inhibits the AKT signaling pathway to activate autophagy and ameliorate TGFB-induced renal fibrosis, *Autophagy*, 2023, **20**, 1114–1133.
4 Z. Liu, W. Wang, X. Li, S. Tang, D. Meng, W. Xia, H. Wang, Y. Wu, X. Zhou and J. Zhang, Capsaicin ameliorates renal fibrosis by inhibiting TGF-β1–Smad2/3 signaling, *Phytomedicine*, 2022, **100**, 154067.
5 J. Zou, X. Zhou, Y. Ma and R. Yu, Losartan ameliorates renal interstitial fibrosis through metabolic pathway and Smurfs-TGF-β/Smad, *Biomed. Pharmacother.*, 2022, **149**, 112931.
6 X. Gao, Y. Yin, S. Liu, K. Dong, J. Wang and C. Guo, Fucoidan-proanthocyanidins nanoparticles protect against cisplatin-induced acute kidney injury by activating mitophagy and inhibiting mtDNA-cGAS/STING signaling pathway, *Int. J. Biol. Macromol.*, 2023, **245**, 125541.
7 Z. Liu, M. Wang, X. Wang, Q. Bu, Q. Wang, W. Su, L. Li, H. Zhou and L. Lu, XBP1 deficiency promotes hepatocyte pyroptosis by impairing mitophagy to activate mtDNA-cGAS-STING signaling in macrophages during acute liver injury, *Redox Biol.*, 2022, **52**, 102305.
8 L.-Y. Chang, Y.-L. Chao, C.-C. Chiu, P.-L. Chen and H. Y. H. Lin, Mitochondrial Signaling, the Mechanisms of AKI-to-CKD Transition and Potential Treatment Targets, *Int. J. Mol. Sci.*, 2024, **25**, 1518.
9 X. Sun, J. Chen, Y. Huang, S. Zhu, S. Wang, Z. Xu, J. Zhang and W. Sun, Yishen Qingli Heluo Granule Ameliorates Renal Dysfunction in 5/6 Nephrectomized Rats by Targeting Gut Microbiota and Intestinal Barrier Integrity, *Front. Pharmacol.*, 2022, **13**, 858881.
10 Q. Jiang, L. Chen, R. Wang, Y. Chen, S. Deng, G. Shen, S. Liu and X. Xiang, Hypoglycemic mechanism of Tegillarca granosa polysaccharides on type 2 diabetic mice by altering gut microbiota and regulating the PI3K-akt signaling pathwaye, *Food Sci. Hum. Wellness*, 2024, **13**, 842–855.
11 H. Wang, A. Ainiwaer, Y. Song, L. Qin, A. Peng, H. Bao and H. Qin, Perturbed gut microbiome and fecal and serum

metabolomes are associated with chronic kidney disease severity, *Microbiome*, 2023, **11**, 3.

12 G. R. Saranya and P. Viswanathan, Gut microbiota dysbiosis in AKI to CKD transition, *Biomed. Pharmacother.*, 2023, **161**, 114447.

13 T. Lan, T. Tang, Y. Li, Y. Duan, Q. Yuan, W. Liu, Y. Ren, N. Li, X. Liu, Y. Zhang, X. Li, G. Jin, S. Wang and J. Guo, FTZ polysaccharides ameliorate kidney injury in diabetic mice by regulating gut-kidney axis, *Phytomedicine*, 2023, **118**, 154935.

14 L. Voroneanu, A. Burlacu, C. Brinza, A. Covic, G. G. Balan, I. Nistor, C. Popa, S. Hogas and A. Covic, Gut Microbiota in Chronic Kidney Disease: From Composition to Modulation towards Better Outcomes—A Systematic Review, *J. Clin. Med.*, 2023, **12**, 1948.

15 L. Qiao, G. Yang, P. Wang and C. Xu, The potential role of mitochondria in the microbiota-gut-brain axis: Implications for brain health, *Pharmacol. Res.*, 2024, **209**, 107434.

16 S. Yuan, Z. Ye, Y. Li, J. Zou, M. Wu, K. Wang, W. Liao and J. Shen, Hypoglycemic Effect of Nobiletin *via* Regulation of Islet β-Cell Mitophagy and Gut Microbiota Homeostasis in Streptozocin-Challenged Mice, *J. Agric. Food Chem.*, 2022, **70**, 5805–5818.

17 Y. Cai, S. Liu, X. Ge, L. Cheng and X. Zhang, Inhibitory effect of tea flower polysaccharides on oxidative stress and microglial oxidative damage in aging mice by regulating gut microbiota, *Food Funct.*, 2024, **15**, 11444–11457.

18 W. Li, H. Chen, H. Chen, Z. Li, W. Hu, Q. Zhou, B. Xu, Y. Wang and X. Xing, Andrias davidianus bone peptides alleviates hyperuricemia-induced kidney damage in vitro and in vivo, *Food Sci. Hum. Wellness*, 2024, **13**, 1886–1905.

19 W. E. Hardman, Walnuts Have Potential for Cancer Prevention and Treatment in Mice, *J. Nutr.*, 2014, **144**, 555S–560S.

20 M. Kornsteiner-Krenn, K.-H. Wagner and I. Elmadfa, Phytosterol Content and Fatty Acid Pattern of Ten Different Nut Types, *Int. J. Vitam. Nutr. Res.*, 2013, **83**, 263–270.

21 S. Bakrim, N. El Omari, E. J. Khan, A. Khalid, A. N. Abdalla, J. B. Chook, K. W. Goh, L. C. Ming, S. Aboulaghras and A. Bouyahya, Phytosterols activating nuclear receptors are involving in steroid hormone-dependent cancers: Myth or fact?, *Biomed. Pharmacother.*, 2023, **169**, 115783.

22 M. C. Brañes, R. Gillet and R. Valenzuela, Efficacy of Submicron Dispersible Free Phytosterols on Non-Alcoholic Fatty Liver Disease: A Pilot Study, *J. Clin. Med.*, 2023, **12**, 979.

23 J. Baek, C. He, F. Afshinnia, G. Michailidis and S. Pennathur, Lipidomic approaches to dissect dysregulated lipid metabolism in kidney disease, *Nat. Rev. Nephrol.*, 2021, **18**, 38–55.

24 F. Yang, L. Sun, Y. Gao, J. Liang, W. Ye, W. Yang, S. Xie, J. Zhou, R. Li and X. Zhou, Integrating Network Pharmacology and Metabolomics to Explore the Potential Mechanism of β–Sitosterol Against Hyperuricemia Nephropathy, *J. Food Biochem.*, 2024, **2024**, 7645677.

25 J. Yang, C. Li, Y. Liu, Y. Han, H. Zhao, S. Luo, C. Zhao, N. Jiang, M. Yang and L. Sun, Using network pharmacology to explore the mechanism of Danggui-Shaoyao-San in the treatment of diabetic kidney disease, *Front. Pharmacol.*, 2022, **13**, 832299.

26 J. Yang and S. Li, Molecular mechanism of Hedyotis Diffusae Herba in the treatment of lupus nephritis based on network pharmacology, *Front. Pharmacol.*, 2023, **14**, 1118804.

27 J. Song, W. Yu, S. Chen, J. Huang, C. Zhou and H. Liang, Remimazolam attenuates inflammation and kidney fibrosis following folic acid injury, *Eur. J. Pharmacol.*, 2024, **966**, 176342.

28 B. Zhu, Y. Ni, Y. Gong, X. Kang, H. Guo, X. Liu, J. Li and L. Wang, Formononetin ameliorates ferroptosis-associated fibrosis in renal tubular epithelial cells and in mice with chronic kidney disease by suppressing the Smad3/ATF3/SLC7A11 signaling, *Life Sci.*, 2023, **315**, 121331.

29 A. O. Antwi, D. D. Obiri, N. Osafo, A. D. Forkuo and L. B. Essel, Stigmasterol inhibits lipopolysaccharide-induced innate immune responses in murine models, *Int. Immunopharmacol.*, 2017, **53**, 105–113.

30 X. Tang, T. Yan, S. Wang, Q. Liu, Q. Yang, Y. Zhang, Y. Li, Y. Wu, S. Liu, Y. Ma and L. Yang, Treatment with β-sitosterol ameliorates the effects of cerebral ischemia/reperfusion injury by suppressing cholesterol overload, endoplasmic reticulum stress, and apoptosis, *Neural Regener. Res.*, 2024, **19**, 642–649.

31 S. Reagan-Shaw, M. Nihal and N. Ahmad, Dose translation from animal to human studies revisited, *FASEB J.*, 2007, **22**, 659–661.

32 R. A. Moreau, L. Nyström, B. D. Whitaker, J. K. Winkler-Moser, D. J. Baer, S. K. Gebauer and K. B. Hicks, Phytosterols and their derivatives: Structural diversity, distribution, metabolism, analysis, and health-promoting uses, *Prog. Lipid Res.*, 2018, **70**, 35–61.

33 M. Wang, W. Huang, Y. Hu, L. Zhang, Y. Shao, M. Wang, F. Zhang, Z. Zhao, X. Mei, T. Li, D. Wang, Y. Liang, J. Li, Y. Huang, L. Zhang, T. Xu, H. Song, Y. Zhong and B. Lu, Phytosterol Profiles of Common Foods and Estimated Natural Intake of Different Structures and Forms in China, *J. Agric. Food Chem.*, 2018, **66**, 2669–2676.

34 R. Yang, L. Xue, L. Zhang, X. Wang, X. Qi, J. Jiang, L. Yu, X. Wang, W. Zhang, Q. Zhang and P. Li, Phytosterol Contents of Edible Oils and Their Contributions to Estimated Phytosterol Intake in the Chinese Diet, *Foods*, 2019, **8**, 334.

35 M. Huang, Y. Yan, Z. Deng, L. Zhou, M. She, Y. Yang, M. Zhang and D. Wang, Saikosaponin A and D attenuate skeletal muscle atrophy in chronic kidney disease by reducing oxidative stress through activation of PI3K/AKT/Nrf2 pathway, *Phytomedicine*, 2023, **114**, 154766.

36 L. Li, M. Lu, Y. Peng, J. Huang, X. Tang, J. Chen, J. Li, X. Hong, M. He, H. Fu, R. Liu, F. F. Hou, L. Zhou and Y. Liu, Oxidatively stressed extracellular microenvironment

drives fibroblast activation and kidney fibrosis, *Redox Biol.*, 2023, **67**, 102868.

37 H. Hu, W. Li, Y. Hao, Z. Peng, Z. Zou and W. Liang, Baicalin ameliorates renal fibrosis by upregulating CPT1α-mediated fatty acid oxidation in diabetic kidney disease, *Phytomedicine*, 2024, **122**, 155162.

38 J. Song, H. Wang, J. Sheng, W. Zhang, J. Lei, W. Gan, F. Cai and Y. Yang, Vitexin attenuates chronic kidney disease by inhibiting renal tubular epithelial cell ferroptosis *via* NRF2 activation, *Mol. Med.*, 2023, **29**, 147.

39 S. Pan, S.-s. Jiang, R. Li, B. Tian, C. -y. Huang, R. Wang, Y.-y. Li, H. Zhu, Y.-f. Yuan and X. Hu, Hong Guo Ginseng Guo (HGGG) protects against kidney injury in diabetic nephropathy by inhibiting NLRP3 inflammasome and regulating intestinal flora, *Phytomedicine*, 2024, **132**, 155861.

40 M. Kayhan, J. Vouillamoz, D. G. Rodriguez, M. Bugarski, Y. Mitamura, J. Gschwend, C. Schneider, A. Hall, D. Legouis, C. A. Akdis, L. Peter, H. Rehrauer, L. Gewin, R. H. Wenger and S. N. Khodo, Intrinsic TGF-β signaling attenuates proximal tubule mitochondrial injury and inflammation in chronic kidney disease, *Nat. Commun.*, 2023, **14**, 3236.

41 Y. Song, J. Wei, R. Li, R. Fu, P. Han, H. Wang, G. Zhang, S. Li, S. Chen, Z. Liu, Y. Zhao, C. Zhu, J. Zhu, S. Zhang, H. Pei, J. Cheng, J. Wu, L. Dong, G. Song, X. Shen and Q. Yao, Tyrosine kinase receptor B attenuates liver fibrosis by inhibiting TGF-β/SMAD signaling, *Hepatology*, 2023, **78**, 1433–1447.

42 L. Li, F. Liu, C. Feng, Z. Chen, N. Zhang and J. Mao, Role of mitochondrial dysfunction in kidney disease: Insights from the cGAS-STING signaling pathway, *Chin. Med. J.*, 2024, **137**, 1044–1053.

43 S. Liu, X. Gao, Y. Yin, J. Wang, K. Dong, D. Shi, X. Wu and C. Guo, Silk fibroin peptide self-assembled nanofibers delivered naringenin to alleviate cisplatin-induced acute kidney injury by inhibiting mtDNA-cGAS-STING pathway, *Food Chem. Toxicol.*, 2023, **177**, 113844.

44 J. Willemsen, M.-T. Neuhoff, T. Hoyler, E. Noir, C. Tessier, S. Sarret, T. N. Thorsen, A. Littlewood-Evans, J. Zhang, M. Hasan, J. S. Rush, D. Guerini and R. M. Siegel, TNF leads to mtDNA release and cGAS/STING-dependent interferon responses that support inflammatory arthritis, *Cell Rep.*, 2021, **37**, 109977.

45 N. Dagar, A. Kale, S. Steiger, H.-J. Anders and A. B. Gaikwad, Receptor-mediated mitophagy: An emerging therapeutic target in acute kidney injury, *Mitochondrion*, 2022, **66**, 82–91.

46 Z. Deng, M. He, H. Hu, W. Zhang, Y. Zhang, Y. Ge, T. Ma, J. Wu, L. Li, M. Sun, S. An, J. Li, Q. Huang, S. Gong, J. Zhang, Z. Chen and Z. Zeng, Melatonin attenuates sepsis-induced acute kidney injury by promoting mitophagy through SIRT3-mediated TFAM deacetylation, *Autophagy*, 2023, **20**, 151–165.

47 J. Li, D. Yang, Z. Li, M. Zhao, D. Wang, Z. Sun, P. Wen, Y. Dai, F. Gou, Y. Ji, D. Zhao and L. Yang, PINK1/Parkin-mediated mitophagy in neurodegenerative diseases, *Ageing Res. Rev.*, 2023, **84**, 101817.

48 J. I. Jiménez-Loygorri, B. Villarejo-Zori, Á. Viedma-Poyatos, J. Zapata-Muñoz, R. Benítez-Fernández, M. D. Frutos-Lisón, F. A. Tomás-Barberán, J. C. Espín, E. Area-Gómez, A. Gomez-Duran and P. Boya, Mitophagy curtails cytosolic mtDNA-dependent activation of cGAS/STING inflammation during aging, *Nat. Commun.*, 2024, **15**, 830.

49 D. A. Sliter, J. Martinez, L. Hao, X. Chen, N. Sun, T. D. Fischer, J. L. Burman, Y. Li, Z. Zhang, D. P. Narendra, H. Cai, M. Borsche, C. Klein and R. J. Youle, Parkin and PINK1 mitigate STING-induced inflammation, *Nature*, 2018, **561**, 258–262.

50 A. Mocanu, R. A. Bogos, T. I. Lazaruc, L. M. Trandafir, V. V. Lupu, I. Ioniuc, M. Alecsa, A. Ivanov, A. Lupu and I. M. Starcea, Exploring a Complex Interplay: Kidney–Gut Axis in Pediatric Chronic Kidney Disease, *Nutrients*, 2023, **15**, 3609.

51 S. Cabała, M. Ożgo and A. Herosimczyk, The Kidney–Gut Axis as a Novel Target for Nutritional Intervention to Counteract Chronic Kidney Disease Progression, *Metabolites*, 2024, **14**, 78.

52 X. Yang, D. Zeng, C. Li, W. Yu, G. Xie, Y. Zhang and W. Lu, Therapeutic potential and mechanism of functional oligosaccharides in inflammatory bowel disease: a review, *Food Sci. Hum. Wellness*, 2023, **12**, 2135–2150.

53 X. Xiao, J. Wang, Y. Zhu, B. Deng, Y. Liu, S. Wang, T. Hou and T. Song, Phytosterols Protect against Osteoporosis by Regulating Gut Microbiota, *J. Agric. Food Chem.*, 2023, **71**, 14539–14549.

54 B. Han, L. Shi, M.-Y. Bao, F.-L. Yu, Y. Zhang, X.-Y. Lu, Y. Wang, D.-X. Li, J.-C. Lin, W. Jia, X. Li and Y. Zhang, Dietary ellagic acid therapy for CNS autoimmunity: Targeting on Alloprevotella rava and propionate metabolism, *Microbiome*, 2024, **12**, 114.

55 X. Lu, C. Guo and Y. Zhu, Selenium-enriched crude polysaccharide from Rosa roxburghii Tratt ameliorates cadmium-induced acute kidney injury in mice by modulating intestinal microorganisms, *Heliyon*, 2023, **9**, e19678.

56 J. Fu, G. Li, X. Li, S. Song, L. Cheng, B. Rui and L. Jiang, Gut commensal Alistipes as a potential pathogenic factor in colorectal cancer, *Discover Oncol.*, 2024, **15**, 473.

57 W. Lei, M. Qi, P. Tan, S. Yang, L. Fan, H. Li and Z. Gao, Impact of polyphenol-loaded edible starch nanomaterials on antioxidant capacity and gut microbiota, *Int. J. Biol. Macromol.*, 2024, **265**, 130979.

